Pair correlations in high-K bands

D. ALMEHED, S. FRAUENDORF AND F. DÖNAU

IKH, FZ Rossendorf, PF 510119, D-01314 Dresden, Germany and Department of Physics, University of Notre Dame, IN 46556, USA

The tilted axis cranking model is used in combination with the random phase approximation and particle number projection to analyze the influence of dynamical pair correlations in the high-K bands of ^{178}W and their effect on relative energy and angular momentum. The calculations show the importance of dynamical pair correlations to describe the experiment as well as advantages and problems with the different models in the superfluid and normal state regions.

PACS numbers: 21.60.-n, 21.60.Jz, 27.70.+q

I. INTRODUCTION

The transition of a nucleus from the superfluid to the normal state at high angular momentum is an interesting problem that is studied by means of modern γ-detector arrays. Contrary to the analogous transition in solids, in the finite nuclear system there is no sharp phase change but an extended transition region with in which pairing effects disappear. The most rapid attenuation of pair correlations is caused by quasiparticle excitations i.e. breaking of pairs. This case is realized in deformed nuclei when a large fraction of the angular momentum is generated along the symmetry axis of the nucleus. These states may appear as high-K isomers near the yrast line. Hence, the experimental data on high-K isomers and the rotational structures built on those states contain valuable information about the pair correlations and how they are influenced by the rotation.

The theoretical analysis of high-K band structures presented in this paper is based on the tilted axis cranking [1] (TAC) model, which is a mean field approach for describing both the rotation and pair correlations in the framework of the Hartree-Fock-Bogoliubov (HFB) theory. In fact, the TAC model has already been applied to the high-K multi-quasiparticle bands in $^{178,179}W$ [2]. There, only the effects of *static* pair field have been considered. The central aim of our present investigation is studying the role of *dynamical* pair correlations. For this purpose we apply the random phase approximation (RPA) to the pairing interaction, which includes the fluctuations of the pair field. The fluctuations are particularly important when the static pair field has collapsed. Their relevance is suggested by the results of [2,3] for $^{178,179}W$ as well as in the earlier investigations of the pair correlations of other high-K band heads states [4].

The combination of the HFB theory with RPA does not provide an reliable description in the region where the pairing gap disappears [5]. There the particle number projection method (PNP) works better [3,6]. Therefore, both methods, RPA and PNP, are considered and compared with each other.

The paper is organized as follows. In section II we develop TAC versions which include pairing-RPA or PNP. Details of the calculations are given in section III. The results of the calculations of high-K bands in ^{178}W are presented in section IV and compared with the experiment [7].

II. THE MODEL

A. Mean field

Our investigations are based on the single particle Routhian [1] of the TAC model complemented by a monopole pair interaction term,

$$\mathcal{H}' = t + V(\varepsilon_\nu) - \omega(\sin\vartheta j_1 + \cos\vartheta j_3) - GP^\dagger P - \lambda\hat{N}, \tag{1}$$

where $P^\dagger$ denotes the monopole pair field operator [5] and $\hat{N}$ is the particle number operator. For simplicity the terms are written only for one kind of particles.

Replacing in $\mathcal{H}'$ the pairing two-body term by the pair potential one obtains the quasiparticle Routhian

$$h' = t + V(\varepsilon_\nu) - \omega(\sin\vartheta j_1 + \cos\vartheta j_3) - \Delta(P^\dagger + P) - \lambda\hat{N}. \tag{2}$$

The diagonalization of h' (for details cf. [5]) provides the quasiparticle energies $e'_i(\omega)$ as well as the HFB amplitudes (u, v), required later on for the RPA and PNP calculations. In order to define a quasiparticle state $| >$ for a specific

configuration the occupation numbers need to be chosen. The self-consistent treatment of h' implies determining the pair gap Δ from the HFB gap equation

$$G < P^\dagger >= \Delta \tag{3}$$

and fixing the chemical potential λ by the particle number condition

$$< \hat{N} >= N. \tag{4}$$

These conditions remain valid for the RPA but they will be modified for the PNP approach (cf. section II C). The HFB part of the total Routhian becomes

$$R_{HFB} =< \mathcal{H}' > +\lambda N. \tag{5}$$

In order to determine the deformation parameters ε_ν we have constructed the Total Routhian Surface (TRS) using the standard Strutinsky renormalization procedure as described e.g. in [8,9]. As shown in [10] the essential shell-correction part $E_{strut}(\varepsilon_\nu)$ of the TRS can be calculated for a non-rotating and unpaired ground state. The contribution containing the dependence on rotation and pair field enters via the quasiparticle Routhian, eq. (5). Hence, the total Routhian can be written as

$$R(\omega, \varepsilon_\nu, \Delta, \lambda, \vartheta) = E_{strut}(\varepsilon_\nu) + R_{HFB}(\omega, \varepsilon_\nu, \Delta, \lambda, \vartheta). \tag{6}$$

B. Pairing-RPA

So far only the mean field part of the pairing energy has been taken into account. Now we include the pair correlation energy, which comes from quantum vibrations around the mean field minimum. The RPA treatment of the pair interaction gives the following expression for the correlation energy [3]

$$E_{corr}^{RPA} = \frac{1}{2} \left[\sum_\nu \Omega_\nu - \sum_\mu E_\mu \right] + E_{ex} \tag{7}$$

where Ω_ν are the RPA frequencies for the pair vibrations, $E_\mu = e_i + e_j$ ($\mu = i < j$) are the two-quasiparticle energies and E_{ex} is the so-called boson exchange term. The total Routhian is the obtained from eqs. (6,7) as

$$R^{RPA}(\omega, \varepsilon_\nu, \Delta, \lambda, \vartheta) = R(\omega, \varepsilon_\nu, \Delta, \lambda, \vartheta) + E_{corr}^{RPA}(\omega, \varepsilon_\nu, \Delta, \lambda, \vartheta). \tag{8}$$

Due to the large number of RPA roots in deformed nuclei, it is practically impossible to evaluate the sum in eq. (7) directly [3,6]. However, it can be calculated by means of the integration method developed recently [11], which is especially simple for pairing interaction. It uses the RPA response function $F(\Omega)$ (cf. [3,5]), which reads explicitly for our case:

$$F(\Omega) = \left(2G \sum_\mu \frac{S_\mu^{+2} E_\mu}{E_\mu^2 - \Omega^2} - 1 \right) \left(2G \sum_\mu \frac{S_\mu^{-2} E_\mu}{E_\mu^2 - \Omega^2} - 1 \right) - \left(2G\Omega \sum_\mu \frac{S_\mu^+ S_\mu^-}{E_\mu^2 - \Omega^2} \right)^2 \tag{9}$$

where

$$S_\mu^\pm = \frac{1}{\sqrt{2}} \sum_k \left\{ \left(u_{ki} u_{\bar{k}j} \pm v_{kj} v_{\bar{k}i} \right) - \left(u_{kj} u_{\bar{k}i} \pm v_{ki} v_{\bar{k}j} \right) \right\} \tag{10}$$

and u, v are the HFB amplitudes. The zeros of the function $F(\Omega_\nu)$ determine the the RPA frequencies, Ω_ν. Continuing the variable Ω into the complex plane z, one defines the spectral function $\frac{F'(z)}{F(z)}$. It has first order poles at Ω_ν and E_μ and it is analytical for all other complex values of z. According to Cauchy's theorem the following integral relation is obtained:

$$\frac{1}{2\pi i} \oint_C dz \ g(z) \frac{F'(z)}{F(z)} = \sum_\nu g(\Omega_\nu) - \sum_\mu g(E_\mu), \tag{11}$$

2

where $g(z)$ is a arbitrary complex function which is analytical within the region enclosed by the integration path C. The roots Ω_ν and the poles E_μ of $F(z)$ lie in the same region. By choosing $g(z) = z$ the RPA correlation energy, eq. (7) becomes

$$E_{corr}^{RPA} = \frac{1}{4\pi i} \oint_C dz\, z \frac{F'(z)}{F(z)} + E_{ex},$$
(12)

where the integration path C goes around the right half of the complex plane. The exchange term is given by

$$E_{ex} = \frac{G}{2} \sum_\mu \left(S_\mu^{+^2} + S_\mu^{-^2}, \right)$$
(13)

as in [3]. The integral in eq. (11) is independent of the path C as long as all poles in the positive plane are enclosed (see Fig. 1). Therefore C can always be chosen in such a way that the spectral function becomes smooth and the integration numerically stable, such that a small number of grid points can be used in the integration.
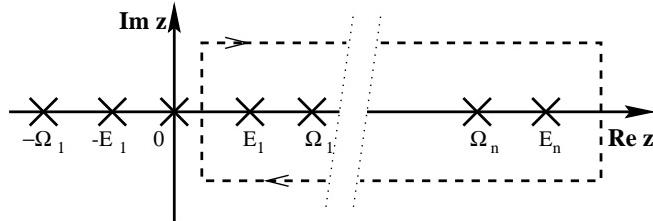

FIG. 1. A schematic picture of the integration contour (dashed line) in the complex plane. The roots Ω_ν and poles E_μ of $F(z)$ are marked with crosses.

The RPA correction to the angular momentum operator [12]

$$J_i^{(2)} = \sum_{ij,kml} j_{km}^i \left(u_{ki}u_{mj} - v_{ki}v_{mj} \right) b_{il}^\dagger b_{jl},$$
(14)

gives us the RPA contribution $< J_i^{(2)}(\Omega_\nu) >$ of the RPA solution Ω_ν, where j_{km}^i are the single particle matrix elements of the angular momentum components $i = x, y, z$ and the term $b_{il}^\dagger b_{jl}$ is the boson image of the two quasiparticle scattering contribution of the angular momentum operator. By choosing the weight function $g(z) = < J_i^{(2)}(z) >$ in the integral, (11) the corresponding RPA contribution to J_i can be calculated too.

It should be pointed out that eq. (7) takes into account also the contribution from possible spurious modes. In the paired case $\Delta > 0$ the function $F(z)$ has a root at $z = 0$. This does not cause a problem for the integration since the factor z in the integrand in eq. (12) cancels this pole. After the transition to $\Delta = 0$ the spurious mode disappears.

The above described method can be straightforwardly applied to obtain the correlation energy of the $K = 0$ ground state band. The RPA for the excited configurations of the high-K bands needs special care concerning the selection of the "physical" phonon modes from the full RPA spectrum $\pm\Omega_\nu$ which implies positive and negative frequencies. The general criterion is to select from the pair of roots $\pm\Omega_\nu$ the one with the positive normalization. Such an identification is trivial for the ground configuration because there all $\Omega_\nu > 0$ have positive normalization. However, for excited configurations the normalization check has to be done explicitly. Since the excited configurations under study are still close to the ground configuration the search for the possible physical phonons with $\Omega_\nu < 0$ can be confined to a narrow energy region of a few MeV above zero. For this region the sum (7) is directly evaluated whereas for the higher lying part the loop integration is done. We mention that the correlation energy is also for excited configurations a negative (gain) term the value of which depends on the rotational frequency as well as on the configuration under study.

In calculating the RPA contribution to the angular momentum components by means of eq. (14), we observed that for some phonons, Ω_ν, the backward going amplitudes become so large that the underlying quasiboson approximation (QBA) of the RPA is no longer valid. This happens in excited configurations near instabilities of the static pair field, which occur when two configurations with different Δ cross each other. Examples are the bands $K = 7, 15$ (neutron pairing) and $K = 15, 22$ (proton pairing), which will be discussed in section IV B. For the low lying RPA solutions we check explicitly whether the QBA condition, $\langle\nu| b_{il}^\dagger b_{jl} |\nu\rangle \ll 1$, is satisfied or not. We exclude roots with $\langle\nu| b_{il}^\dagger b_{jl} |\nu\rangle > 0.1$ from the sum (14).

This procedure may be justified as follows. In the extended boson approximation (EBA) [13,14] the non zero term $\langle\nu| b_{il}^\dagger b_{jl} |\nu\rangle$ is approximatively taken into account by an iterative process. The relevant effect of the EBA as compared

to QBA is a strong reduction of the backward going amplitudes [14]. A full EBA treatment is too demanding for a realistic calculation like ours. Instead we use the rough approximation that the backward going amplitudes are quenched in the cases when QBA is not valid. i.e. if $\langle \nu | b_{il}^\dagger b_{jl} | \nu \rangle > 0.1$ the roots are removed from the sum (14) of the RPA correction. These roots would give a very large (several units of $\hbar$) contribution to the angular momentum. If they are included, J_{RPA} changes very rapidly near the crossings between configurations with different Δ. It is known the cranking model is unreliable near such crossings, where it seems justified to resort to an only rough correction of the QBA, which results in a smooth reasonable function $J_{RPA}(\omega)$.

C. Particle number projection

The above treatment of the dynamical pair correlations by combining the HFB and RPA methods does not work for $\Delta \to 0$. Another approximate method to include the dynamical pair correlations is the particle number projection (PNP) [3,5]. In the PNP approach a variational state $|N >$ with good particle number N is formed by applying the projection integral

$$|N > \propto \int_0^{2\pi} d\phi \; e^{-i\phi(\hat{N} - N)} | > \tag{15}$$

to a TAC eigenstate $| >$ of the quasiparticle Routhian h', eq. (2). Number projection accounts for gauge angle fluctuations of the pair field on a circle in the complex plane ($\Delta e^{-i\phi}$) with the radius Δ, but disregards radial fluctuations.

The PNP energy function to be minimized is the expectation value

$$R_{PNP}(\Delta) = < N | \mathcal{H}' | N > + \lambda N \tag{16}$$

calculated with the projected state $|N >$, eq. (15). We do not perform a full variation of the HFB amplitudes of the reference state $| >$ but minimize the energy (16) only with respect to the variable gap parameter Δ. The minimization of eq. (16) in PNP replaces the self-consistency condition (3) for calculating Δ in the HFB approach. Compared to the self-consistent pair gap (denoted by Δ^{HFB} in the following) of an unprojected quasiparticle state, the pair gap Δ^{PNP} optimizing the projected Routhian (16) is generally larger and stays non-zero through the phase transition region.

In the HFB variant of TAC, the constraint $< \hat{N} >= N$ adds an additional dimension to the system of nonlinear equations given by eq. (3) and the minimization with respect to ε_ν and ϑ. Performing the PNP the above condition is automatically satisfied. Instead λ becomes another variable parameter of the Ritz variational problem, which is to be determined by minimizing the Routhian. However, the minimum practically coincides with the solution of eq. (4), as illustrated in Fig. 2. This has the advantage that in the vicinity of the minimum the energy does not change very much. Thus the errors remain small if the minimum in λ is not exactly found (or eq. (4) is not exactly solved). Keeping λ fixed greatly simplifies the actual calculation. However, one has to be careful that fixing λ does not affect the general properties of the configuration too much. As will be discussed in Appendix A, neglecting the exchange term of the interaction may lead to problems in calculating the projected energy. Unlike the unprojected HFB function $| >$, the projected wave function (15) is not be stationary. This may lead to problems that will be discussed in section II D.
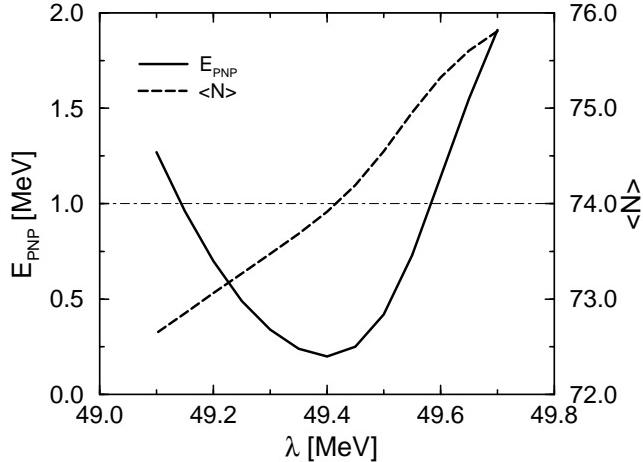
FIG. 2. Particle number expectation value in the unprojected case, $< N >$, and the total energy in the projected case, E_{PNP}, as functions of λ. This example corresponds to the yrast neutron configuration at $\omega = 0.4$ (MeV). The correct particle number $< N >$ is represented by a horizontal dot-dashed line.

D. Energy minimum in ϑ

Since the shell correction part in total Routhian R, eq. (6), does not depend on the tilt angle ϑ one has

$$\frac{\partial R}{\partial \vartheta} = \frac{\partial}{\partial \vartheta} \langle h' \rangle = \left\langle \frac{\partial h'}{\partial \vartheta} \right\rangle + 2 < |h' \frac{\partial}{\partial \vartheta}| > . \qquad (17)$$

The term $< |h' \frac{\partial}{\partial \vartheta}| >$ vanishes because $| >$ is a stationary eigenstate to h'. Hence, the derivative of the Routhian becomes

$$\frac{\partial R}{\partial \vartheta} = \left\langle \frac{\partial h'}{\partial \vartheta} \right\rangle = -\omega \left(\cos \vartheta < J_1 > - \sin \vartheta < J_3 > \right) = -\omega J_\perp. \qquad (18)$$

Thus, the requirement $\frac{\partial R}{\partial \vartheta} = 0$ for the minimization is cast into the condition $J_\perp = 0$. In other words, $\vec{\omega}$ and $\vec{J}$ must be parallel [1].

In case of particle number projection, the state $|N >$ is not an eigenstate to h' and eq. (18) is not strictly valid. The energy minimum will no longer exactly agree with the condition of parallelity, which is the condition for uniform rotation. In the PNP calculations the minimum condition $\frac{\partial R}{\partial \vartheta} = 0$ needs to be fulfilled even if $J_\perp = 0$ is not satisfied.

We generally found small differences ($0° - 10°$) between the values of ϑ obtained from the condition $J_\perp(\omega) = 0$ and the energy minimum. Substantial deviations appear in regions of band crossings, where the cranking model is unreliable [15] anyway, and sometimes close to the band head.

III. DETAILS OF THE CALCULATIONS

We use the modified oscillator model with deformations ε_2, ε_4 and standard Nilsson parameters [16]. The high-K bands in nucleus ^{178}W are found to be axially symmetric configurations. The tilt angle ϑ is the angle between the symmetry (3-)axis and the rotational axis. The Strutinsky part $E_{strut}(\varepsilon_\nu)$ of the TRS, eq. (6) is obtained practically by including 8 oscillator shells for protons and neutrons, respectively. For calculating the quasiparticle term R_{TAC}, eq. (5), it is sufficient to consider only a few shells around the Fermi surface. We included in the diagonalization of the quasiparticle Routhian the four N-shells closest to the Fermi surface. It is important to follow a certain quasiparticle configuration when seeking the minimum of $R(\omega, \varepsilon_2 \varepsilon_4, \Delta, \lambda, \vartheta)$. This is achieved by 'diabatic tracing': When changing one of the parameters determining h' the overlap of the quasiparticle wave functions with the ones before the step is calculated. By looking for the maximal overlap a one-to-one correspondence between the quasiparticle states is established. Figure 3 shows a quasiparticle diagram constructed in this way by using the step size $\Delta\omega = 0.05$ MeV, $\Delta\vartheta = 5°$. Keeping the occupation of such diabatic quasiparticle trajectories one usually follows a quasiparticle

5

configuration of a given structure. Problems may appear near quasi-crossings like the ones in Fig. 3 where the configurations are mixed up.
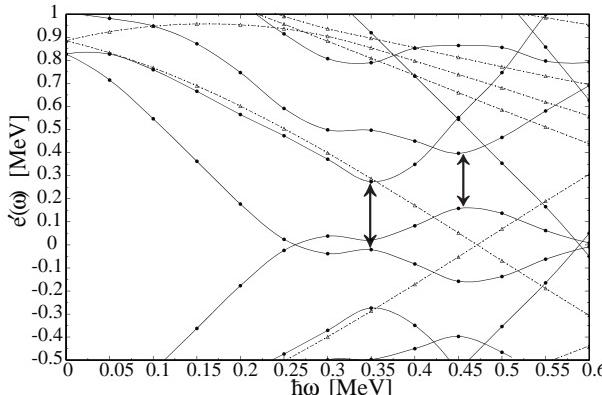

FIG. 3. A quasiparticle diagram. The lines are connected by diabatic tracing, i.e. by finding the largest overlap between the points of two successive values of ω. Solid lines correspond to quasiparticles with positive parity while the dot-dashed ones have a negative parity. Two quasi crossings are marked with double arrows.

We have used two different strategies for finding the minimum with respect to Δ and ϑ for different ω.

1. (a) Construct the configuration for $\Delta = 0$. Choose a reasonable start value ϑ_S for different ω.
   (b) Find minimum in ϑ by tracing diabatically for fixed Δ.
   (c) Find minimum in Δ by tracing diabatically for fixed ϑ.
   (d) Iterate by returning to (b) until total minimum is found.

2. (a) Construct the configuration for the band head for a guessed Δ.
   (b) Find minimum for Δ.
   (c) Go to the next ω-point with fix Δ, tracing diabatically.
   (d) Vary Δ and ϑ as in 1b - 1d.
   (e) Iterate by returning to (c)

Usually 1. is better to work with because the minimum in ϑ does not change much when pairing is added. Strategy 2. is more appropriate for the ground configuration, because it has no counterpart in the case of zero pairing.

The equilibrium shape of ^{178}W turned out to be rather stable. The deformation differs by less then 5% between different band heads (cf. [17]). We also found that the deformation changes very little within the bands. Thus, we adopted the fixed deformations $\varepsilon_2 = 0.229$ and $\varepsilon_4 = 0.034$ calculated for the ground state. These values were used for all bands except $K^\pi = 25^+$. This band contains a $h_{9/2}$ aligned proton, which drives the equilibrium values to $\varepsilon_2 = 0.255$ and $\varepsilon_4 = 0.038$. The relative energy of the bands is sensitive to the strength of the pairing force G [17]. In our calculations, G was fixed to match the values of the even-odd mass differences as calculated with PNP [18].

$$\Delta_\nu = 1.15 \text{ MeV} \rightarrow G_\nu = 0.093 \text{ MeV}$$

$$\Delta_\pi = 1.23 \text{ MeV} \rightarrow G_\pi = 0.121 \text{ MeV}$$

In the PNP calculation the value of λ is determined for each configuration at $\omega = 0.4$ (MeV) by minimizing $R(\lambda)$ and kept constant for each configuration. In RPA and HFB calculations, λ is adjusted according to eq. (4) for each configuration and ω, because the HFB energy is much more sensitive to this parameter.

IV. RESULTS

The configurations of the considered K-bands are listed in table I. They are in accordance with [7]. The following presentation is divided into two parts. The first part treats the cases where HFB gap Δ^{HFB} has collapsed already at

the band head ($K^\pi = 25^+$ and 30^+) while second comprises the cases where the pair field has transitional character ($K^\pi = 7^-$, 15^+ and 22^-).

For a given configuration, there is usually only a weak systematic reduction of Δ when ω increases. It only changes substantially when a pair of protons or neutrons becomes aligned at a band crossing in a configuration with a low number of excited quasiparticles. For example, in the yrast band there is a drastic decrease of Δ_ν through the crossing region at $\omega_c \approx 0.3$. It is well known [15] that the cranking model has problems close to a band crossing. In this region, the different strategies (cf. section III) of optimizing the mean-field parameters can result in different configurations and, as a consequence, in different self-consistent values of the parameters. In our TAC calculations for K-bands, we observed the general tendency that the tilt angle ϑ increases monotonically from $0°$ at the band head to a value close to $\vartheta = 90°$ at highest frequency. In some cases there is a decrease in ϑ at high $\omega(> 0.5)$, which can be related to the crossing with other configurations.

K^π	Neutron configuration	Proton configuration
7^-	$\nu\{7/2^+, 7/2^-\}$	
15^+	$\nu\{7/2^+, 7/2^-\}$	$\pi\{7/2^+, 9/2^-\}$
22^-	$\nu\{5/2^-, 7/2^+, 7/2^-, 9/2^+\}$	$\pi\{7/2^+, 9/2^-\}$
25^+	$\nu\{5/2^-, 7/2^+, 7/2^-, 9/2^+\}$	$\pi\{1/2^-, 5/2^+, 7/2^+, 9/2^-\}$
30^+	$\nu\{5/2^-, 7/2^+, 7/2^-, 9/2^+\}$	$\pi\{5/2^+, 7/2^+, 9/2^-, 11/2^-\}$

TABLE I. Occupied orbitals (Ω^π) of the multi quasiparticle excitations (K^π). The quasiparticle configurations are taken from [7]. Complete assignment: Neutrons $5/2^-[512], 7/2^+[633], 7/2^-[514], 9/2^+[624]$ and protons $1/2^-[541], 5/2^+[402], 7/2^+[404], 9/2^-[514], 11/2^-[505]$

A. $K^\pi = 25^+$ and 30^+

In these eight-quasiparticle configurations the static pair field has disappeared ($\Delta^{HFB} = 0$). The pair correlations are only of dynamical nature. One can expect the RPA to do a good job in describing them because one is sufficiently away from the critical region. As mentioned above, the PNP calculation leads to a finite value of Δ^{PNP} which is 30% smaller then the values in the ground state (c.f. Fig. 4 and 5). There is a weak reduction towards higher ω within each band.
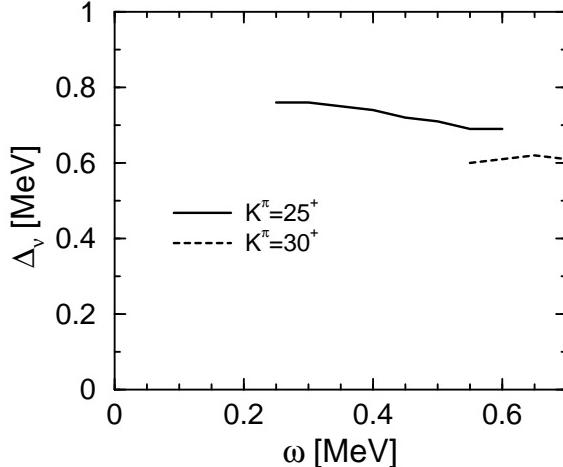
FIG. 4. Δ^{PNP} as a function of ω for neutrons in the $K^\pi = 25^+$ and 30^+ bands. Note, in these cases is $\Delta^{HFB} = 0$.
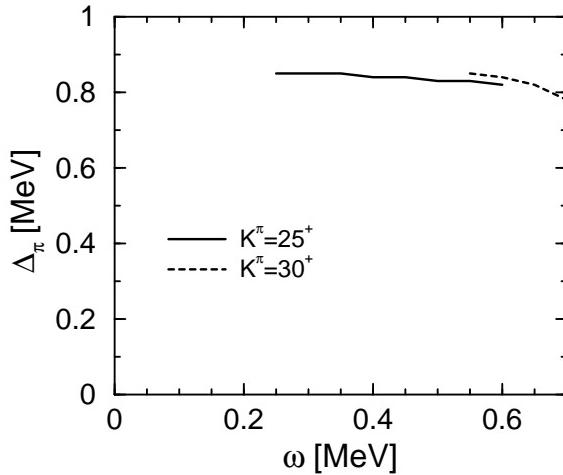
FIG. 5. Δ^{PNP} as a function of ω for protons in the $K^\pi = 25^+$ and 30^+ bands. Note, in these cases is $\Delta^{HFB} = 0$.

1. Routhians

Experimental Routhians are calculated by means of the standard expressions given e.g. in [19]. In order to remove the steep decrease of $R(\omega)$ a term $30 MeV^{-1}\omega^2$ is added to all R values, which makes the differences between the various curves better visible. The calculated ground state energy $R_{g.s.}(\omega = 0)$ is set to zero for all calculations and the experiment. The PNP and RPA calculations give an energy gain relative to the HFB results. Due to the blocking effect, this gain is normally smaller in the excited states than in the ground state. As a consequence the energy relative to the ground state gets larger for RPA and PNP than for HFB calculations. This systematic tendency is substantiated by the examples to be shown.

For the $K^\pi = 25^+$ band the RPA yields a substantially better agreement with experiment than PNP (cf. Fig. 6). The larger discrepancy for the $K^\pi = 30^+$ may reflect some inaccuracy of single particle levels. Although the HFB

calculation gives a good estimate of the angular momentum [2] it underestimate the relative energy of the bands. The rotational frequency of the band head is also quite well reproduced by RPA and PNP.
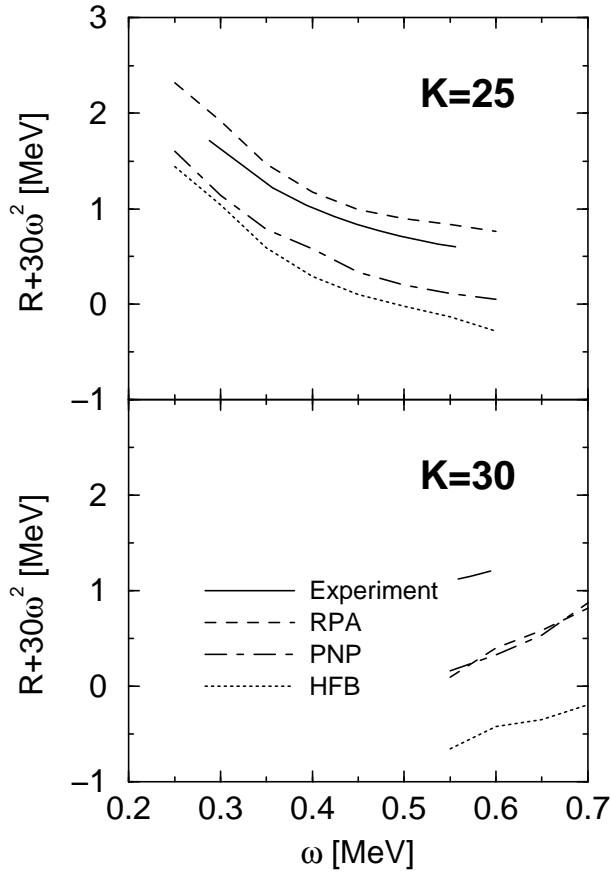

FIG. 6. The energies in the rotating frame $R(\omega)$ relative to the ground state for the $K^\pi = 25^+$ (upper) and $K^\pi = 30^+$ (lower) bands. A term of $30\omega^2$ is added to the R values. The experimental values are taken from [7].

In Fig. 7 the energy differences between the paired (PNP or RPA) and unpaired calculation (Hartree-Fock) are shown. They characterize the effect of the pair correlation onto the energy. We can see that the RPA gives a larger pair correlation energy then PNP in accordance with [20]. This indicates that the RPA is a better approximation than PNP in the $\Delta^{HFB} = 0$ regime. One notices that the correlation energy is only weakly reduced by rotation.
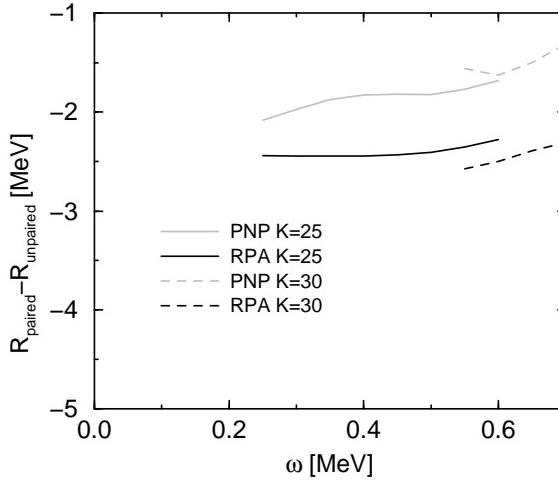
FIG. 7. The total pair correlation energies in the rotating frame $R_{paired}(\omega) - R_{unpaired}$ for the the $K^\pi = 25^+$ and 30^+.

The investigation [2] demonstrated that the angular momentum and the dynamical moment of inertia of ^{178}W can be understood by assuming that the nucleons move in a rotating mean field with no pairing. The strong reduction of the moment of inertia as compared to the rigid body[1] value is due to the nuclear shell structure (cf. [2] and section IV C). As seen in Fig. 8, the inclusion of dynamic pair correlations does not change this result. Note that a linear term has been subtracted so that the differences between the curves are considerably magnified.
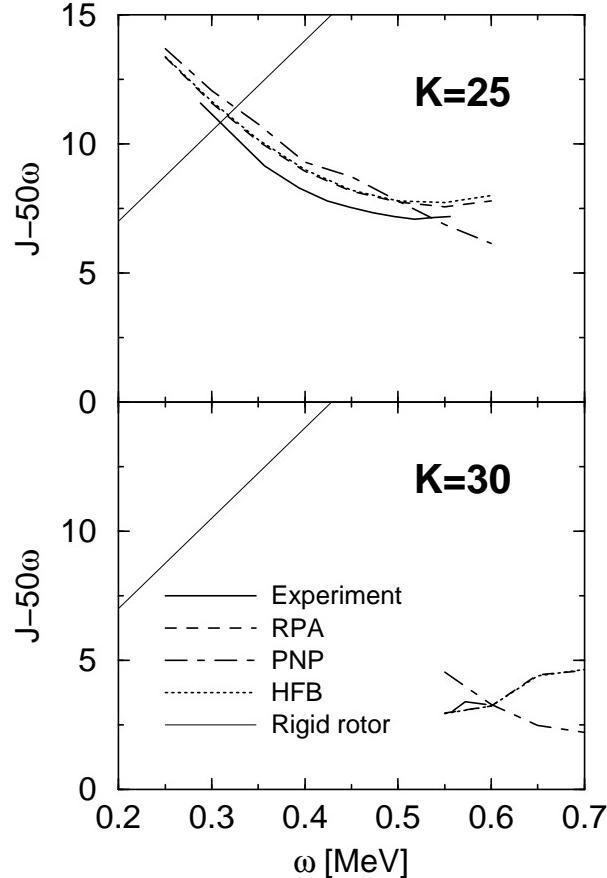
FIG. 8. Angular momentum $J(\omega)$ for $K^\pi = 25^+$ and 30^+. A term of 50ω is subtracted from the J values. The experimental values are taken from [7]. The RPA and HFB results practically coincide in this picture.

All approaches reproduce the experimental dynamical moment of inertia ($\mathcal{J}^{(2)} = \frac{dJ}{d\omega}$) which is substantially below the rigid body value. The differences of the function $J(\omega)$ between paired and the unpaired calculations are only marginal. The dynamical pair correlations do not change the angular momentum very much, but they do increase the energy difference between bands with a different number of blocked quasiparticles.

3. Branching ratios

In the TAC model, the $B(M1)$ and $B(E2)$ values are calculated by means of the expressions

$$B(M1) = \frac{3}{8\pi} \left[\sin\vartheta \left(J_{3\pi} + 2.35S_{3\pi} - 2.24S_{3\nu} \right) - \cos\vartheta \left(J_{1\pi} + 2.35S_{1\pi} - 2.24S_{1\nu} \right) \right]^2 \tag{19}$$

---

[1]This limit is referred to the rotational spectrum $E(I) = A_{rig}I(I+1) - K^2$.

and

$$B(E2) = \frac{15}{128\pi} \left(\sin\vartheta\right)^4 Q_0^2 \tag{20}$$

where J, S and Q_0 are the expectation values of the angular momentum, the spin and the quadrupole moment, respectively, as calculated with the TAC states. It is common practice to present the experimental branching ratios in the form $\left|\frac{(g_K - g_R)}{Q_0}(\omega)\right|$, which is obtained assuming that the strong coupling limit [21] is valid. We choose to display the calculated branching ratios (which of course do not rely on the strong coupling assumption) in the same way. The theoretical ratios are obtained as

$$\left|\frac{(g_K - g_R)}{Q_0}(\omega)\right| = \sqrt{\frac{5}{16}} \sqrt{\frac{1}{K^2} - \frac{1}{J^2}} \sqrt{\frac{B(M1)}{B(E2)}} \tag{21}$$

where K, the value of the angular momentum at the band head, is kept constant and J is the calculated value of the angular momentum. Q_0 is chosen as in [7].
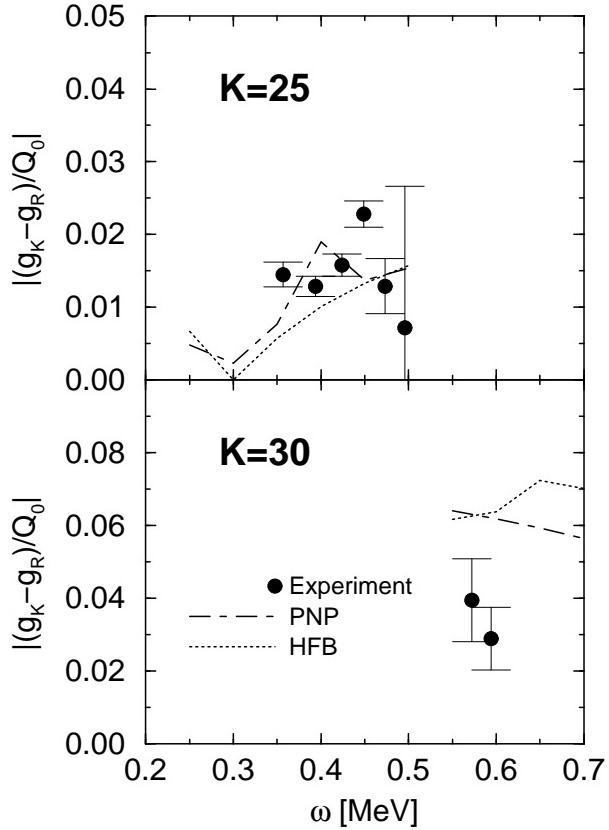

FIG. 9. The ratio $\left|\frac{(g_K - g_R)}{Q_0}(\omega)\right|$ for the $K^\pi = 25^+$ and 30^+ bands. The experimental values are taken from [7]. Observe the different scales.

The theoretical and experimental ratios are given in Fig. 9. Since the ratio depends strongly on the orientation of the proton and neutron angular momentum the good agreement confirms our calculated geometry. The experimental errors of the branching ratios are too large to discriminate between the PNP and HFB calculation.

B. $K^\pi = 7^-$, 15^+ and 22^-

The $K^\pi = 7^-$, 15^+ and 22^- bands are analyzed and presented in the same way as the $K^\pi = 25^+$ and 30^+ bands. These bands, which correspond to the excitation of two to six quasiparticles from the $K = 0$ ground configuration,

11

have a reduced but non-zero static HFB pair field at the band head. The PNP is expected to be stable while the RPA can run into problems since one is close to the transition $\Delta^{HFB} \to 0$.
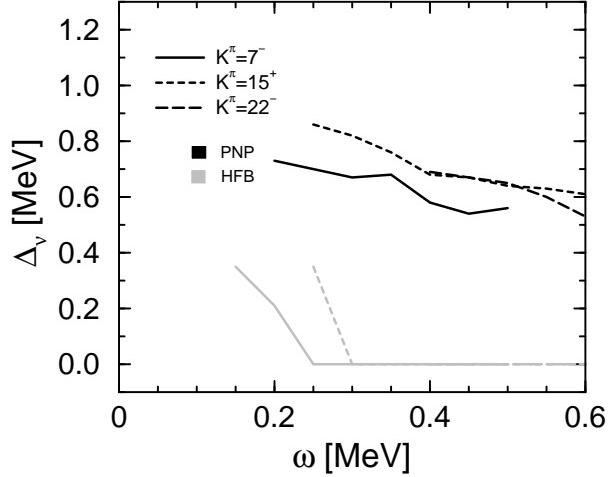

FIG. 10. Δ^{HFB}(grey) and Δ^{PNP}(black) as a function of ω for neutrons in the $K^\pi = 7^-$, 15^+ and 22^- bands.
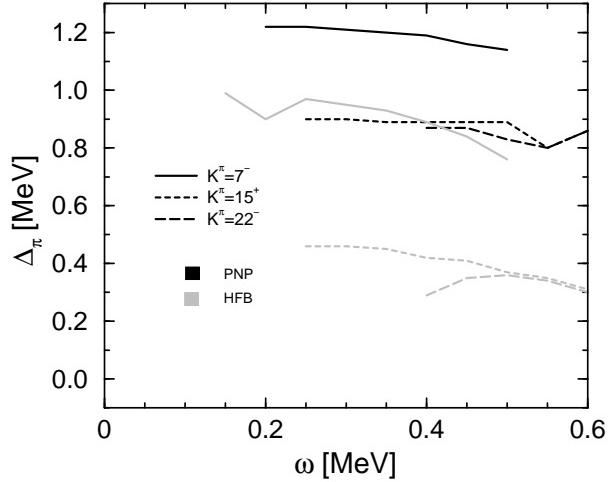
FIG. 11. Δ^{HFB}(grey) and Δ^{PNP}(black) as a function of ω for protons in the $K^\pi = 7^-$, 15^+ and 22^- bands.

Figure 10 and 11 show the calculated values of Δ. The values of Δ^{PNP} are similar to the ones for the $K^\pi = 25^+$ and 30^+ bands in Figs. 4 and 5, except $K^\pi = 7^-$, for which the protons remain in the ground configuration. For the two quasi neutron bands $K^\pi = 7^-$ and 15^+ the gap Δ_ν^{HFB} is reduced strongly already at the band head and becomes zero at $\omega \approx 0.3$ (MeV). These values indicate that the pair filed is nearly instable, which causes problems to be be discussed in section IV B 2. Though Δ_π^{HFB} is strongly reduced in the two quasi proton configurations $K^\pi = 15^+$ and 22^- it changes only weakly with ω.

1. Routhians

Both the PNP and RPA calculations fairly well reproduce the Routhians at high ω. There, again the tendency is seen that the dynamical pair correlations enlarge the energy distance between the bands. The exception is the $K^\pi = 15^+$ for $\omega > 0.38$ MeV. This discrepancy will be discussed in section IV B 2.
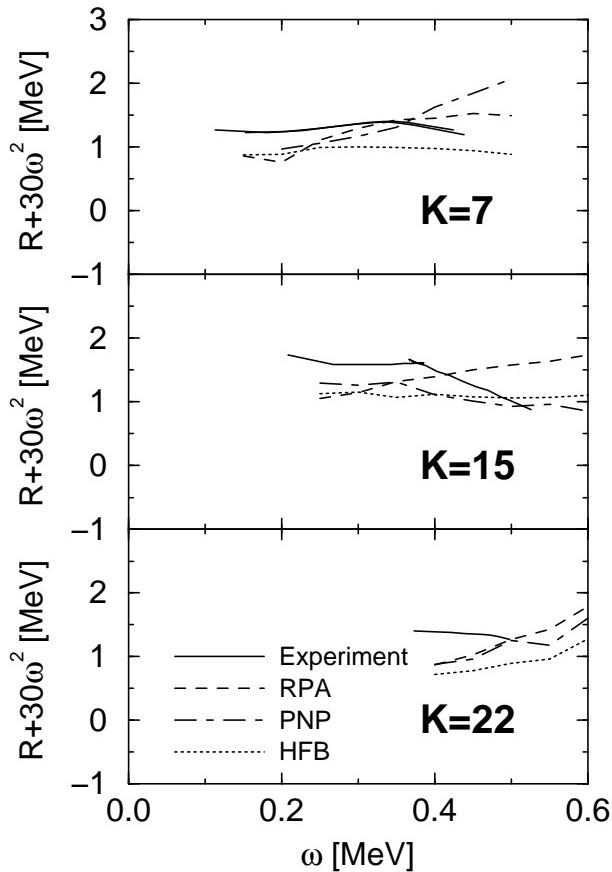
FIG. 12. The energies in the rotating frame $R(\omega)$ relative to the ground state for the $K^\pi = 7^-$ (upper), 15^+ (middle) and 22^- (lower) bands. A term of $30\omega^2$ is added to the R values. The experimental values are taken from [7].

Figure 13 shows that the pair correlation energies for these lower K values are larger and depend stronger on the rotational velocity than the ones in Fig. 7. The HFB + RPA calculations cannot reproduce the backbend in the $K^\pi = 7^-$ and 15^+ bands since $\Delta_\nu^{HFB} = 0$ for $\omega > 0.25$ MeV. It is seen as the kink in Fig. 12 and the upbend of the PNP calculation in Fig. 13. The erratic behavior of the PNP pairing energy at large ω can be understood by the fact that the energy surface has a shallow minimum and is therefore easily disturbed by structure effects caused by quasiparticle crossings. Most of these crossings do not exist in the HFB + RPA calculations because $\Delta_\nu^{HFB} = 0$. As a consequence, R depends more smoothly on ω, as the experiment does. We consider the fluctuations of R as an error of the PNP approach, which mimics the dynamical correlations by a static Δ^{PNP}.
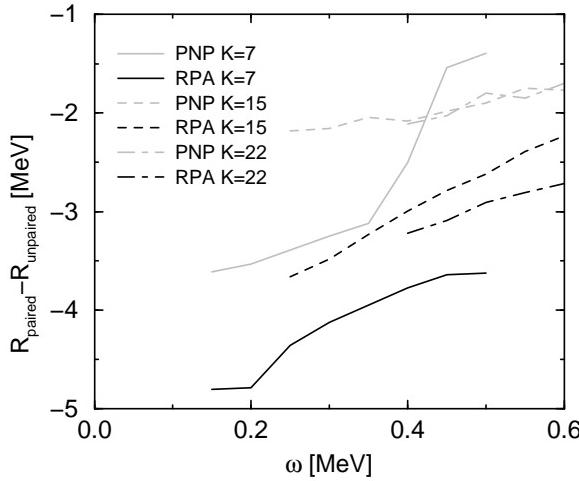
FIG. 13. The total pair correlation energies in the rotating frame $R_{paired}(\omega) - R_{unpaired}$ for the the $K^\pi = 7^-$, 15^+ and 22^-.

2. Angular momentum

As seen in Fig. 14, the calculations give reasonable agreement with the experiment. The neutron backbends in the $K^\pi = 7^-$ and 15^+ are not reproduced in the HFB + RPA calculation because the static pair gap collapses already before the backbend. This feature could be corrected by using a somewhat larger pairing strength G_ν. The PNP calculation gives approximately the right value of ω_c for the neutron backbend but gives a slightly too low value of $J(\omega)$ for the $K^\pi = 7^-$ band.

In the $K^\pi = 15^+$ band, all the calculations underestimate the angular momentum by $\sim 5\hbar$ after the backbend at $\omega \sim 0.38$ MeV. We assign this increase to a configuration change caused by a crossing between a $h_{9/2}$ proton orbital and a $h_{11/2}$ proton orbital. As a result a $K^\pi = 19^+$ band continues the $K^\pi = 15^+$ band. This crossing occurs at the same ω as the neutron crossing causing the normal backbend. The same proton crossing occurs in the $K^\pi = 22^-$ band at $\omega \sim 0.48$ MeV which continues as a $K^\pi = 26^-$ band. It is seen in Fig. 14 as an upbend. The configurations of the $K^\pi = 19^+$ and 26^- bands are listed in table II. The calculations for the $K^\pi = 7^-$ band after the backbend also gives a bit too low angular momentum. It cannot be explained by the proton crossing discussed. This may indicate that the missing angular momentum in the $K^\pi = 15^+$ and 22^- bands has another origin than suggested above.
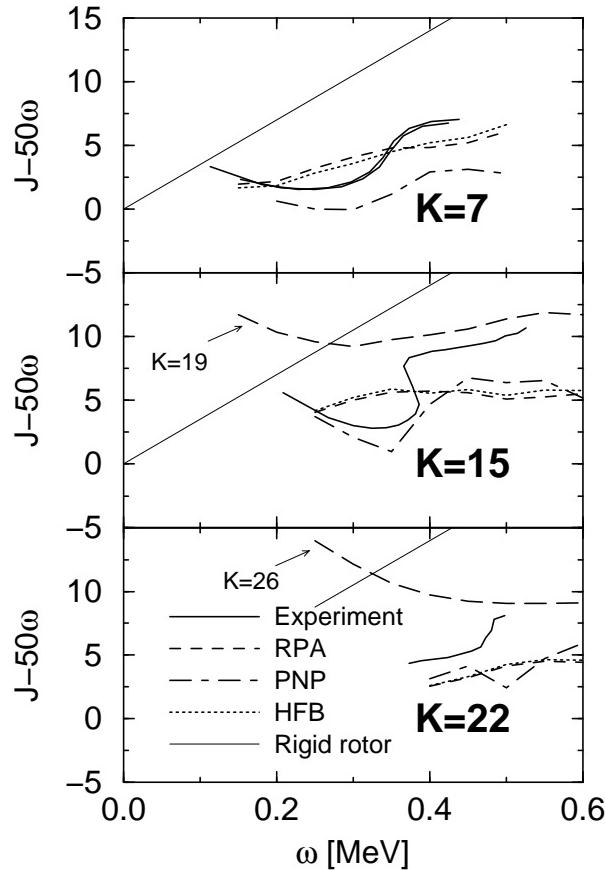

FIG. 14. Angular momentum $J(\omega)$ for $K^\pi = 7^-$, 15^+ and 22^-. The RPA solution for the $K^\pi = 19^+$ (middle) and $K^\pi = 26^-$ (lower) are added. A factor of 50ω is subtracted from the J values. The experimental values are taken from [7]. The RPA and HFB results practically coincide in this picture.

K^π	Neutron configuration	Proton configuration
19^+	$\nu\{7/2^+, 7/2^-\}$	$\pi\{1/2^-, 7/2^-, 7/2^+, 9/2^-\}$
26^-	$\nu\{5/2^-, 7/2^+, 7/2^-, 9/2^+\}$	$\pi\{1/2^-, 7/2^-, 7/2^+, 9/2^-\}$

14

TABLE II. The quasiparticle configurations used in the article are taken from [7]. (Neutrons: $5/2^-[512], 7/2^+[633], 7/2^-[514], 9/2^+[624]$ Protons: $1/2^-[541], 7/2^-[523], 7/2^+[404], 9/2^-[514]$)

The good agreement with experiment in Fig. 15 for the $K^\pi = 15^+$ and 22^- confirms the geometry of our calculations. Again, the large experimental errors of the branching ratios do not allow to distinguish between the PNP and HFB calculations.
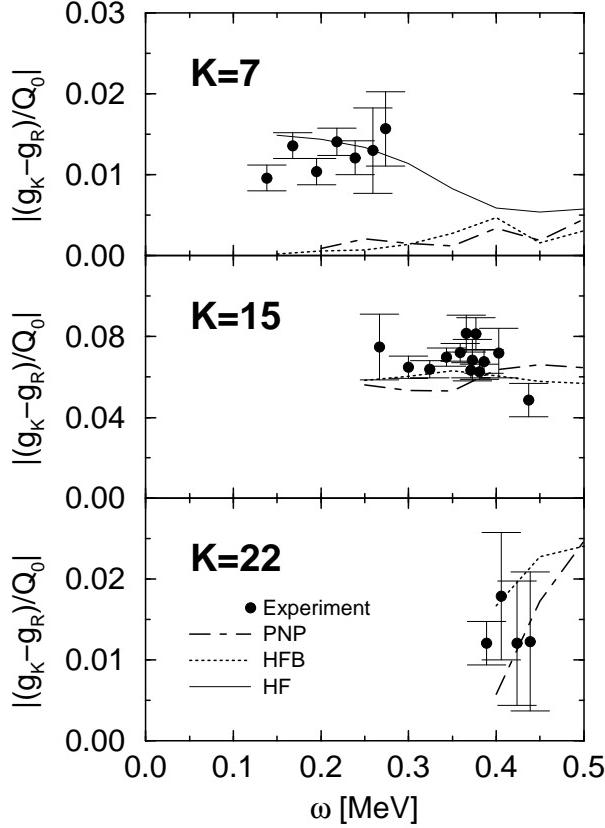

FIG. 15. The ratio $|\frac{(g_K - g_R)}{Q_0}(\omega)|$ for the $K^\pi = 7^-$ (upper), 15^+ (middle) and 22^- (lower) bands. The thin full line (HF) displays the case $\Delta = 0$ for comparison. The experimental values are taken from [7]. Observe the different scales.

In the case of the $K^\pi = 7^-$ band, the calculation with $\Delta = 0$ reproduces the branching ratios better. We consider this as accidental, because the presence of the upbend seen in the $I(\omega)$ curve of Fig. 14 is a clear indication of a finite pairing gap for the neutrons. The protons are definitely in their ground configuration with a non-zero gap. The $K^\pi = 7^-$ band has small $B(M1)$ values compared to other K-bands. This is expected because the normally dominating proton contributions to the $B(M1)$ value (19) are small for the ground configuration and very sensitive to the size of Δ_π, It is largely canceled by the negative neutron spin contribution. Hence, the resulting ratio is not reliable.

C. COMPARISON OF ALL K-BANDS

In Figs. 16–18 we compare the Routhians and the angular momenta of different K-bands at a fixed frequency $\omega = 0.45$ MeV. The $K = 30$ band is left out from the plots since it starts at a higher ω. The bands with different orientation of $\vec{J}$ have approximately the same energy R in the rotating frame. Their energies in the laboratory frame for a given value of J do not differ much as well. That is so, because the energy needed for generating angular momentum along the two principal axes 1 and 3 is nearly the same. This feature, which is reflected by many bands with different orientation being close to the yrast line, is characteristic for the (N,Z) region where ^{178}W is situated.
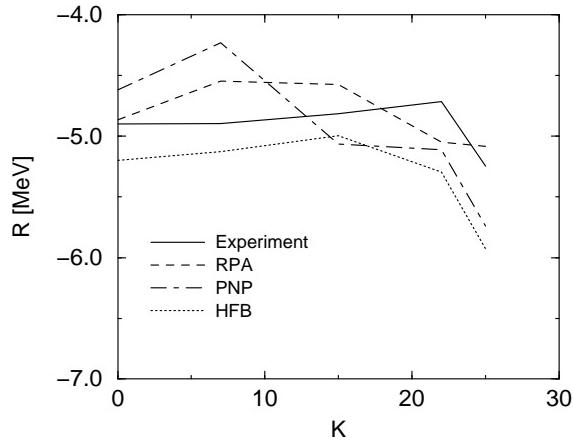
FIG. 16. The energies in the rotating frame relative to the ground state as a function of K for $\omega = 0.45$. The K-values plotted are 0 (s-band), 7, 15, 22 and 25. The experimental values are taken from [7].
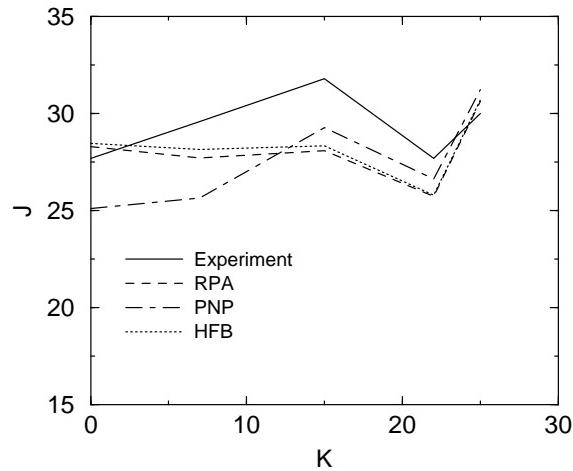

FIG. 17. The angular momentum as a function of K for $\omega = 0.45$. The K-values plotted are 0(s-band), 7, 15, 22 and 25. The experimental values are taken from [7].
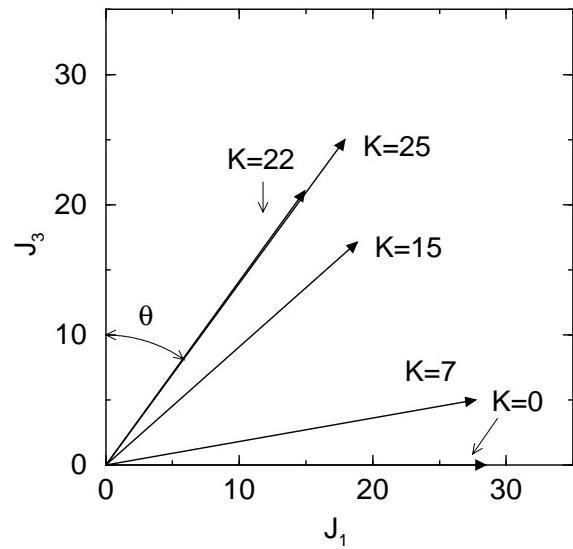
FIG. 18. The angular momentum component along the 1- and 3-axis for different K at $\omega = 0.45$ as calculated with HFB. The K-values plotted are 0(s-band), $7, 15, 22$ and 25.
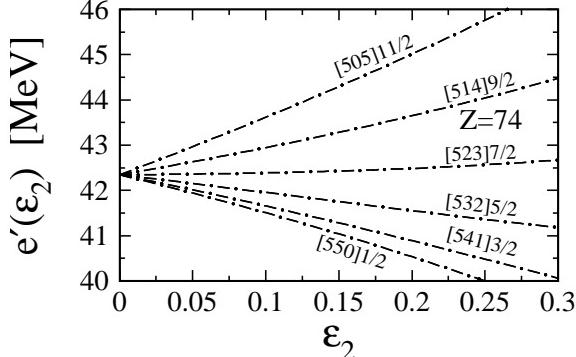

FIG. 19. The negative parity states in the 50–82 protons shell. The larger gaps between the levels in the upper part of the shell promote deformation alignment of angular momentum. The levels are labeled with the asymptotic quantum numbers $[Nn_z m_l]\Omega$.

In the upper and middle part of the 50–82 proton and 82–124 neutron shells there are many orbitals with higher Ω values that strongly couple to the prolate deformed potential whereas the low-Ω orbitals are occupied. Figure 19 shows the $h_{11/2}$ orbitals as an example. For the high-Ω orbitals the Coriolis coupling between states with Ω and $\Omega+1$, which generate a contribution to J_1, is weak, because the energy distance is large and the coupling matrix-element ($\sim \sqrt{j^2 - \Omega^2}$) is small. This is very different from the nuclei situated at the bottom of the shell. For the low-Ω orbitals the energy distance is small and the coupling matrix element large. Hence it is easy to generate a contribution to J_1. Thus, the strong coupling suppresses the angular momentum alignment along the collective 1-axis, which causes the reduction of the moment of inertia relative to the rigid body value.

On the other hand, it is energetically favorable to generate a contribution to J_3, because there are many orbitals with a large $|\Omega|$ near the Fermi surface and it does not cost much energy to generate a particle-hole excitation with a large $K = \Omega_p - (-\Omega_h)$. At the bottom of the shell these excitations cost much more energy, because the orbitals with large $|\Omega|$ are far away. The net result is that at the beginning of the rare earth region the moment of inertia is larger than the rigid body value and generating angular momenta along the 3 axis is unfavorable. In the *upper part* of the region, the moment of inertia is smaller than the rigid body value and generating angular momenta along the 1 and 3 axis is equally favorable (see [2] and [22]). The inclusion of pairing does not change this conclusion.

Figure 18 shows the J_1 and J_3 components for different K-bands calculated with HFB at a typical frequency $\omega = 0.45$. Within $\pm 2\hbar$, the component J_3 is equal to K which means that all bands are not far from the strong coupling regime. The largest deviation is found in the $K = 15$ band where $J_3 \approx 17$ at $\omega = 0.45$. This is an effect of the configuration mixing in the neutron system, which is induced by quasi crossings in a region of high quasiparticle level density. The total spin J is almost independent of K, in accordance with the discussion above. Generating the components J_1 and J_3 of angular momentum costs a comparable amount of energy. The slightly different behavior of the $K = 25$ band is due to extra rotational alignment from the aligning $h_{9/2}$ proton orbital, see discussion in [2].

Summarizing our calculations concerning an improved treatment of pairing we find that i) the conclusions of earlier work [2] can be confirmed and ii) the angular momentum $J(\omega)$ is insensitive to the pair correlations in the frequency region after the first band crossing. This is at variance with the results of [3,6] for low-K bands, where a reduction of several units of angular momentum by the dynamical pair correlations was found. The reason is that the single particle orbits near the Fermi surface, which contribute most to the collective angular momentum, are blocked for the pair correlation by generating the high K. The ratio $|\frac{(g_K - g_R)}{Q_0}(\omega)|$ is also reasonably well reproduced which support the calculated tilted geometry of our solutions.

V. CONCLUSIONS

We included dynamical pair correlations into the tilted axis cranking approach in two different ways: The pairing-RPA method, which allows for harmonic vibrations on top of the HFB mean field, and the particle number projection which describes the dynamical correlations by an increased static pair gap in conjunction with projection onto good particle number. We studied the high K-bands in ^{178}W by means of both methods. As known from investigation of the band head energies [4], the HFB approach tends to underestimate the energetic separation between the bands.

Inclusion of the dynamic correlations improves the energy of bands with zero static pair correlations relative to each other and to the bands with pronounced static pair correlations. When the static pair field is substantial we could not find a systematic improvement of the relative energy due to the dynamical pair correlation. This seems to be in contrast to the result for $K = 0$ bands in [3,6].

The pronounced reduction of the moment of inertia of high-K bands relative to the rigid body value, seen in the experiment, is not due to the pair correlations. It is caused by orbitals close to the Fermi surface which in the mid and upper part of its shell is disfavoring the generation of angular momenta perpendicular to the symmetry axis. It is typical for this region, that the generation of angular momentum along the symmetry axis by particle-hole excitation is equally favorable as compared to the rotational alignment i.e. collective rotation along the perpendicular axis (see [2] and [22]). The inclusion pair correlations, both static and dynamic, does not significantly affect this feature of high-K bands, which is in stark contrast to low-K bands.

In bands where the static pair gap of the HFB treatment has collapsed to zero the RPA method is simpler to use than PNP because there is no need to minimize the Routhian with respect to the Δ and λ parameters. The pair gap introduced in these PNP calculations causes irregularities in the energy and angular momentum which are caused by quasiparticle band crossings. The RPA method, which does not have these crossings, describes the experimental results better. Thus, we consider the irregularities appearing in PNP as an artifact of the approximation and RPA superior in this region. On the other hand, when the HFB mean field pair gap is reduced but not yet zero the RPA method has problems because of its deficiencies near the transition to zero pairing. In these cases it turns out to be important to check the quality of the quasiboson approximation when calculating the RPA contribution to the angular momentum. The PNP method is more stable in these cases.

[1] S. Frauendorf, Nucl. Phys. **A557** 259c (1993); Nucl. Phys. **A 677** 115 (2000); Rev. Mod. Phys. (1999) in press

[2] S. Frauendorf, K. Neergård, J. A. Sheikh and P. M. Walker Phys. Rev. C **61** 064324

[3] Y. R. Shimizu, J. D. Garrett, R. A. Broglia, M. Gallardo and E. Vigezzi, Rev. Mod. Phys. **61** 131 (1989)

[4] K. Jain, O. Burglin, G. D. Dracoulis, B. Fabricius, N. Rowley, and P. M. Walker, Nucl. Phys. **A591**, 61 (1995)

[5] P. Ring and P. Schuck, *The Nuclear Many-Body Problem*, Springer-Verlag, New York 1980

[6] R. A. Broglia, M. Diebel, S. Frauendorf, and M. Gallardo, Phys. Lett. **B166**, 252 (1986)

[7] C. S. Purry, P. M. Walker, G. D. Dracoulis, T. Kibédi, F. G. Kondev, S. Bayer, A. M. Bruce, A. P. Byrne, W. Gelletly, P. H. Regan, C. Thwaites, O. Burglin, and N. Rowley, Nucl. Phys. **A632**, 229 (1998); D. M. Cullen, S. L. King, A. T. Reed, J. A. Sampson, P. M. Walker, C. Wheldon, F. Xu, G. D. Dracoulis, L. Y. Lee, A. O. Machiavelli, R. W. MacLeod, A. N. Wilson, and C. Barton, Phys. Rev. C **60**, 064301 (1999)

[8] K. Neergård, V. V. Pashkevich and S. Frauendorf, Nucl. Phys. **A262**, 61 (1976)

[9] Z. Szymański, *Fast Nuclear Rotation*, Oxford University Press, Oxford 1983

[10] T. R. Werner and J. Dudek, Atomic Data and Nuclear Data Tables **59**, 1 (1995)

[11] F. Dönau, D. Almehed and R. G. Nazmitdinov, Phys. Rev. Lett. **83**, 280 (1999)

[12] R. G. Nazmitdinov, Sov. J. Nucl. Phys. **46**(3), 267 (1987)

[13] K. Hara, Prog. Theor. Phys. **32**, 88 (1964)

[14] K. Ikeda, T. Udagawa, and H. Yamaura, Prog. Theor. Phys. **33**, 22 (1965)

[15] I. Hamamoto, Nucl. Phys. **A271**, 15 (1976)

[16] S. G. Nilsson and I. Ragnarsson, *Shapes and Shells in Nuclear Structure*, Cambridge 1995

[17] F. R. Xu, P.M. Walker, J.A. Sheikh and R. Wyss, Phys. Lett. B**435**, 257 (1998)

[18] S. Frauendorf, Nucl. Phys. **A263**, 150 (1976)

[19] S. Frauendorf, Z. Phys. A**358**, 163c (1997)

[20] K. Hagino and G. F. Bertsch, nucl-th/0003016v2

[21] A. Bohr and B. Mottelson, *Nuclear Structure I*, Benjamin, New York 1969

[22] V. V. Pashkevich and S. Frauendorf, Yad. Fiz. **20**, 1122 (1975) [Sov. J. Nucl. Phys. **20**, 588 (1975)]

[23] F. Dönau, Phys. Rev. C**58**, 872 (1998)

APPENDIX A: THE ROLE OF THE EXCHANGE TERM IN PARTICLE NUMBER PROJECTION

The HFB pairing energy is usually calculated in Hartree approximation, i.e. neglecting the exchange term by factorizing the pairing matrix element $< P^\dagger P > \approx < P^\dagger >< P >$. This approximation is justified for the calculation of the pairing energy contribution without PNP. However, it was recently suggested [23] that the neglect of exchange terms in performing PNP can lead to dangerous poles in the resulting total Routhian surface (TRS) Such an unphysical behavior of the PES was indeed found in our calculations and it was traced back to the above mentioned factorization. For the sake of completeness we sketch the argumentation presented in more detail in [23].

Using in the construction of the PNP state $|N>$ eq. (15) and the canonical (BCS-like) form [5] of the HFB state $|>$, the number projected pairing energy $E_{pair} = -G < N|P^\dagger P|N >$ can be written as the sum

$$E_{pair} = E_{pair}^{Direct} + E_{pair}^{Exchange}, \tag{A1}$$

where the direct term

$$E_{pair}^{Direct} = -G < N|N >^{-1} \int d\varphi \left[\sum_{k>0} \frac{2P_{k\bar{k}}v_k u_k e^{i\varphi}}{(u_k^2 + v_k^2 e^{2i\varphi})} \right]^2 < \varphi = 0|\varphi > . \tag{A2}$$

and the usually neglected exchange term

$$E_{pair}^{Exchange} = -G < N|N >^{-1} \int d\varphi \sum_{km} \frac{2P_{km}^2 v_k^2 v_m^2 e^{4i\varphi}}{(u_k^2 + v_k^2 e^{2i\varphi})(u_m^2 + v_m^2 e^{2i\varphi})} < \varphi = 0|\varphi > . \tag{A3}$$

These expressions contain the canonical BCS-amplitudes u_k, v_k of the quasiparticle state and the matrix elements $P_{kk'}$ of the pair operator in the canonical basis. The bracket

$$< \varphi = 0 \,|\, \varphi > \equiv \Pi_{k>0} (u_k^2 + v_k^2 e^{2i\varphi}). \tag{A4}$$

is the overlap function between gauge rotated quasiparticle states.

One may encounter a zero denominator $(u_k^2 + v_k^2 e^{2i\varphi})$ in both energy terms (A2,A3) e.g. for $u_k = v_k$ and $\varphi = \frac{\pi}{2}$. This is because the double zero in the denominator cannot be canceled by the corresponding single zero in the overlap $< \varphi = 0|\varphi >$, eq. (A4). However, when summing up the two contributions (A2,A3) to the full pairing energy E_{pair} such unphysical poles do exactly cancel.
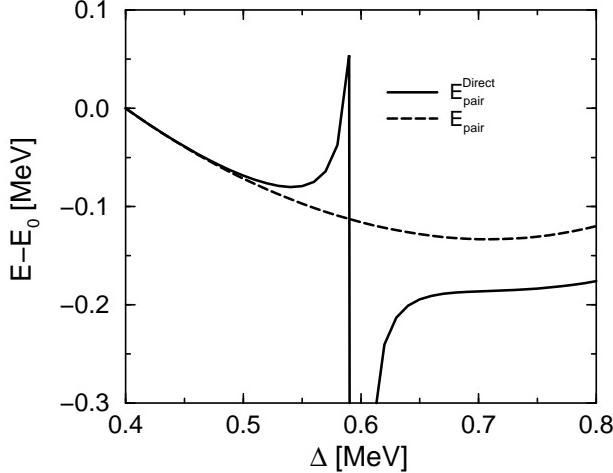

FIG. 20. The energies E_{pair} and the E_{pair}^{Direct} calculated for $\omega = 0.3$ in the $K^\pi = 7^-$ band with $\lambda_N = 49.54$. Both curves are normalized to zero at $\Delta = 0.4$.

Our calculations confirm the conclusion that a reliable calculation of the TRS with PNP has to be done with the full expression. In Fig. 20 the full neutron energy is shown as a function of the neutron gap (Δ) and it is compared to the one where only the direct pairing energy term (A2) is taken into account. The full energy has the expected parabolic shape with the minimum whereas the curve of the direct term alone displays an unphysical pole around $\Delta \approx 0.6$ MeV.
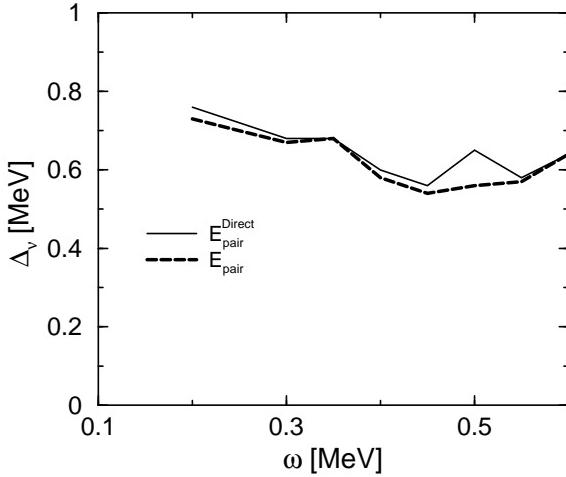
FIG. 21. Δ determined from E_{pair}^{direct} and E_{pair}, respectively, for the $K^\pi = 7^-$ band, see also Fig. 4 and 10. There is only a small difference except at $\omega = 0.5$ where there is a pole in the energy function E_{pair}^{direct}, see Fig. 20. These values of Δ were found keeping all other parameters constant at the self-consistent values found using the full projection.
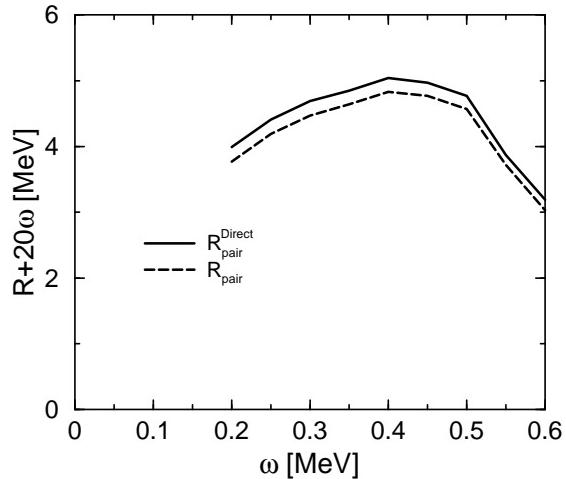

FIG. 22. Routhians R calculated with E_{pair}^{direct} and E_{pair}, respectively, for the $K^\pi = 7^-$ band, see also Fig. 12. There is only a marginal difference between both Routhians where all other parameters are kept constant at the self-consistent values found using the full projection.

Such a strange behavior does not happen often and usually there is only a minor difference between the extracted Δ-value at the minimum for the full and direct energy (cf. Fig. 21). Observables like the energy are not strongly affected by the exchange term except close to poles (cf. Fig. 22). With the full pairing energy, we obtain a minimum for a slightly different Δ and, therefore, a different G is needed to match the experimental Δ-values. We found that a G_π of 0.121 MeV instead of 0.119 MeV should be used for the protons while the G_ν did not change when using the full expression for the pairing energy.

The probability of accidentally hitting a pole is not large but it happened a couple of times in our calculations. The tail (cf. Fig. 20) of a pole can also affect the results and this is, of course, much harder to detect. The energy surface calculated with only the direct term jumps when passing through the pole. This is because a pole has gone in (or out) to the area in the complex plane around which we are integrating. The pole would turn into a step function if it was possible to perform the integration exactly. In order to avoid such unphysical one should generally apply the full expression of the PNP pairing energy.